J Electroceram (2012) 28:178–184
DOI 10.1007/s10832-012-9703-x

Effects of post-treatments on the electrochemical properties of solid-state reacted $Li_4Ti_5O_{12}$—high energy milling and annealing

Jin-Wook Shin · Ji Heon Ryu · Joayoung Jeong · Dang-Hyok Yoon

Received: 11 January 2012 / Accepted: 28 February 2012 / Published online: 23 March 2012

Abstract This study is designed and performed to verify whether nano-sized $Li_4Ti_5O_{12}$ particles can be acquired by simple high energy milling from the economic solid-state reacted coarse powder for high power lithium ion battery applications. For this, $Li_4Ti_5O_{12}$ is synthesized by heat treatment at 800 and 850°C for 3 h using Li_2CO_3 and TiO_2, followed by high energy milling. Even though a comparable particle size to that of expensive wet chemical methods, or even a smaller particle size of 25 nm, can be acquired by 5 h of milling, the electrochemical properties of the particles are found to be deteriorated due to the decrease in $Li_4Ti_5O_{12}$ crystallinity associated with the milling. On the other hand, a subsequent annealing at 750°C for the milled powder is shown to recover both the capacity and rate capability of the anode electrode owing to the increased crystallinity, indicating the importance of particle crystallinity besides a fine particle size for the enhanced electrochemical properties for high power applications.

Keywords Lithium titante · Solid-state reaction · Crystallinity · Electrochemical properties

J.-W. Shin · D.-H. Yoon (✉)
School of Materials Science and Engineering,
Yeungnam University,
Gyeongsan 712-749, South Korea
e-mail: dhyoon@ynu.ac.kr

J. H. Ryu
Graduate School of Knowledge-based Technology & Energy,
Korea Polytechnic University,
Siheung 429-793, South Korea

J. Jeong
Cell Precedence Development Group, Samsung SDI,
Yongin 446-577, South Korea

1 Introduction

Lithium ion batteries have been widely used as power sources for portable electronic devices [1]. Even though the graphite anode material currently used shows acceptable properties for low power applications, it is known to have weaknesses with the high rate capabilities that are essential for the hybrid electric vehicle (HEV) and large-scaled energy storage applications [2–5]. Therefore, extensive research efforts have been made to develop alternative materials that show good cycle performances and excellent high rate properties. In these aspects, a spinel-type lithium titanate ($Li_4Ti_5O_{12}$) with the theoretical capacity of 175 $mAhg^{-1}$ could be a promising anode material for high power applications due to its structural stability with "zero-strain" during the Li^+ intercalation and de-intercalation process as well as its fast charging capabilities [6–11]. In addition, $Li_4Ti_5O_{12}$ does not show a metallic lithium formation on the electrode surface because of its high Li insertion potential of 1.55 V [7, 12], while a graphite anode is known to form a lithium layer due to the low intercalating voltage of approximately 0.05 V (vs. Li/Li^+), especially at fast charging condition [13, 14]. Therefore, the possible safety problems associated with graphite anode, such as combustion or explosion originating from the highly reactive lithium metal plated on the surface, could be effectively avoided by adopting the $Li_4Ti_5O_{12}$ anode.

The most economic method for $Li_4Ti_5O_{12}$ synthesis is a solid-state reaction using TiO_2 and Li_2CO_3, which generally results in a significant amount of agglomeration and a coarse particle size. To achieve a better high rate performance, however, a fine active material is desirable due to its short Li^+ diffusion path and enhanced electrode-electrolyte contact area for fast Li^+ intercalation and de-intercalation [15–18]. For example, it was reported that the nano-sized

$Li_4Ti_5O_{12}$ offered at least a 30 % improvement in rate capability at 1–10 C in a hybrid cell [15, 16]. Consequently, wet chemical methods such as hydrothermal and coprecipitation have been attempted despite their high cost [19-25]. On the other hand, the recent introduction of high energy milling facilities has enabled an efficient reduction in the particle size of starting materials and hence a reduction in synthesized powder. Compared to a conventional ball mill, the modern high energy mill shows significantly higher milling efficiency owing to its high speed rotor, turning at up to several thousand rotations per minute. The high energy input of the high energy mill along with the use of small grinding media, enables the achievement of very small particle sizes in a short processing time [26, 27]. Therefore, examining the possibility for the synthesis of nano-sized particles from a coarse solid-state reacted $Li_4Ti_5O_{12}$ by high energy milling is worthwhile to realize an economic synthesis of nano-sized anode material.

From this background, this study examined the evolution of particle properties in high energy milling using the coarse solid-state reacted $Li_4Ti_5O_{12}$ as well as the electrochemical properties of the resultant anode materials. In addition, the effects of subsequent annealing, which was performed to increase the crystallinity of the milled-powder, on the electrochemical properties were also examined.

2 Experimental

A coarse Li_2CO_3 (D_{mean}=3.80 μm, purity>99.9 %, New Well, Korea) and a very fine TiO_2 (D_{mean}=25 nm, purity> 99.5 %, Evonik, Germany) were used as a Li- and Ti-precursor, respectively, for the solid-state synthesis of $Li_4Ti_5O_{12}$. TiO_2 was composed of 87 % anatase–13 % rutile phase based on Reitveld analysis.

To synthesize 200 g of $Li_4Ti_5O_{12}$ powder, 65.06 g of Li_2CO_3 and 173.68 g of TiO_2, which corresponds to a Li/Ti stoichiometric ratio of 4.05/5.00, were mixed with 400 g of deionized water after adding 2 wt.% of the ammonium salt of polycarboxylic acid (Cerasperse 5468-CF, San Nopco, Korea) with respect to the ceramic powder, as a dispersant. This slight excess in Li from the stoichiometric Li/Ti=4/5 was determined based on the preliminary test, considering the Li evaporation during the high temperature treatment. The formulated mixture was exposed to high-energy milling (MiniCer, Netzsch, Germany) for 3 h at a rotor speed of 3,000 rpm with 0.4 mm ZrO_2 beads, followed by drying at 100°C in a rotary evaporator for uniform mixing. Forty grams of the dried mixture was heat-treated at 800°C, while the remaining mixture was heat-treated at 850°C for 3 h in air at a heating rate of 3°Cmin^{-1}. The $Li_4Ti_5O_{12}$ synthesized at 800°C was named R800C3h and was used as a reference sample in this study. On the other hand, $Li_4Ti_5O_{12}$ synthesized at 850°C was named 850C3hr, where a significant part (100 g) of this sample was used for further experiments. In order to examine the particle size reduction upon milling, a 50 g 850C3hr $Li_4Ti_5O_{12}$ sample was high energy-milled for 1 h, and was named b-HEM1hr. At the same time, a 50 g 850C3hr sample was high energy-milled for 5 h and named b-HEM5hr. Finally, half of the b-HEM5hr was annealed at 750°C for 2 h and named d-750C2hr. The names of the 5 types of $Li_4Ti_5O_{12}$ samples prepared in this study and their treatment histories are summarized in Table 1.

The morphologies of the starting materials, heat-treated and high energy-milled powders were characterized by scanning electron microscopy (SEM: S-4800, Hitachi, Japan) and a HR-STEM (Tecni G^2 F20 S-TWIN, FEI, USA) operated at 200 keV. The evolution of the mean particle size was measured using a particle size analyzer (PSA: Delsa Nano, Beckman Coulter, USA). Since PSA was not able to provide exact data on the primary particle size due to the necking and agglomeration of the powders, the average primary particle size was measured with SEM images for at least 100 particles simultaneously by using image analyzer software (SigmaScan, Systat Software, USA). Room temperature XRD (X'Pert-PRO MPD, PANalytical, The Netherlands) using a Cu K_α line and Rietveld refinement were performed for quantitative phase verification. In addition, Raman spectra (LabRam HR, Horiba, Japan) were excited at 0.5 mW by an Ar^+ laser for the synthesized powders.

To evaluate the electrochemical properties, an electrode paste composed of 80 wt.% $Li_4Ti_5O_{12}$, 10 wt.% acetylene black (Denka black, Denka, Japan) and 10 wt.% poly(vinylidene fluoride) (PVdF, KF1300, Kureha, Japan) was mixed and dispersed. The paste was then screen-printed on Al foil to form an electrode. The electrode plate was then pressed to enhance the inter-particle contact and to ensure a better adhesion to the current collector. Coin-type half-cells (CR2032) were assembled with the composite electrode, Li foil as a counter electrode, and polyethylene film as a separator. The electrolyte used was 1.3 M $LiPF_6$ dissolved in a mixture of ethylene carbonate and ethylmethyl carbonate with a volume ratio of 3:7. The cell assembly was performed in a glove box filled with Ar gas, and the electrode was dried under vacuum at 120°C to remove the moisture before filling the electrolyte. The galvanostatic charge–discharge measurements were performed in a potential range of 1.0–2.5 V (vs. Li/Li^+) at different current conditions of 0.1 *C* (17.5 mAg^{-1}) – 10.0 *C* (1,750 mAg^{-1}). The cells were charged and discharged for three cycles at each current density at 25°C.

3 Results and discussion

Since a solid-state reaction occurs at the contact points of the starting materials, uniform dispersion of starting materials is very important for enhancing the reaction rate and

Table 1 Names of $Li_4Ti_5O_{12}$ synthesized samples with the description on their treatments

No.	Name	Treatments
(a)	R800C3hr	Reference sample. Heat-treated at 800°C for 3 h
(b)	850C3hr	Heat-treated at 850°C for 3 h
(c)	b-HEM1hr	High energy-milled for 1 hr after heat treatment at 850°C for 3 h
(d)	b-HEM5hr	High energy-milled for 5 h after heat treatment at 850°C for 3 h
(e)	d-750C2hr	Annealed at 750°C, 2 h after 850°C, 3 h treatment and 5 h of high energy milling

decreasing the processing temperature. According to the SEM images of the starting materials shown in Fig. 1 (a) and (b), Li_2CO_3 has a large particle size of 3.80 μm, while anatase-rich TiO_2 has a very fine particle size of 25 nm.

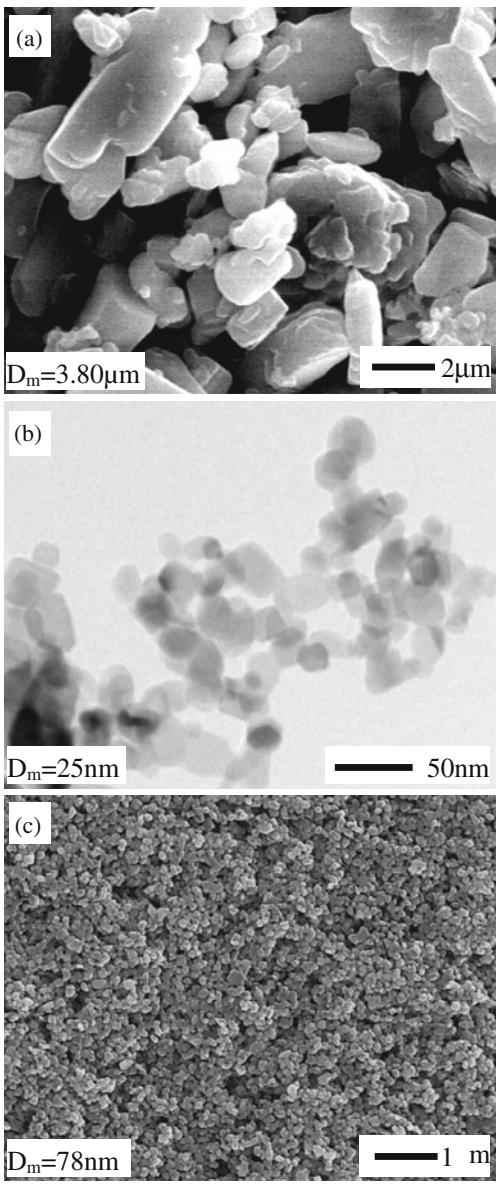

Fig. 1 Electron microscope images of the starting (**a**) Li_2CO_3, (**b**) anatase-rich TiO_2 and (**c**) their mixture after 3 h of high energy milling

Figure 1 (c) shows the Li_2CO_3–TiO_2 mixture after 3 h of high energy milling, whereby finely-milled uniform particles with the mean size of 78 nm can be found, indicating the efficient milling for the coarse Li_2CO_3.

Figure 2 shows the SEM images of the $Li_4Ti_5O_{12}$ samples synthesized by various treatments along with the mean particle size measured using image analyzer software. By heat treatment at 800°C for 3 h, agglomerated $Li_4Ti_5O_{12}$ with a mean particle size of 192 nm was obtained, while the size increased to 353 nm by increasing the temperature to 850°C, as shown in Fig. 2 (a) and (b), respectively. One hour of high energy milling for the 850C3hr sample resulted in broad particle size distribution, which is composed of a few tens of nanometer- and submicrometer-sized $Li_4Ti_5O_{12}$ particles, as shown in Fig. 2 (c). Figure 2 (d) shows that the particle size could be further decreased by increasing the milling time to 5 h. Even though the relatively large-sized particles seemed to be present after 5 h of milling, as marked with the rectangle in Fig. 2 (d), they were found to be the agglomerates of very fine primary particulates of approximately 25 nm, according to the magnified image shown in Fig. 2 (f). Even though the exact mean particle sizes of the high energy-milled $Li_4Ti_5O_{12}$ could not be measured due to the existence of agglomerates using SEM images, the XRD sizes were 38 and 25 nm based on the Scherrer equation for the b-HEM1hr and b-HEM5hr, respectively. When the b-HEM5hr sample was annealed at 750°C for 2 h, the $Li_4Ti_5O_{12}$ particles grew to the mean size of approximately 100 nm, as shown in Fig. 2 (e). Due to the necking and agglomeration of the powders, however, PSA revealed the particle size of 281±31, 497±235, 322±119, 192±63 and 246±31 nm for the powders shown in Fig. 2 (a)–(e), respectively. Even though the particle sizes by PSA were shown to be larger than those by image analyzer, the same trend for both measurements was found upon milling and further heat treatment. Overall, the coarse $Li_4Ti_5O_{12}$ synthesized by solid-state reaction at 850°C could be milled to approximately 25 nm by 5 h of high energy milling, which is comparable to, or even smaller than the sizes obtained using wet chemical methods [19–25].

Figure 3 shows the XRD patterns of the 5 types of $Li_4Ti_5O_{12}$ samples, confirming a pure $Li_4Ti_5O_{12}$ without any trace peaks of rutile TiO_2. Actually, the intermittent

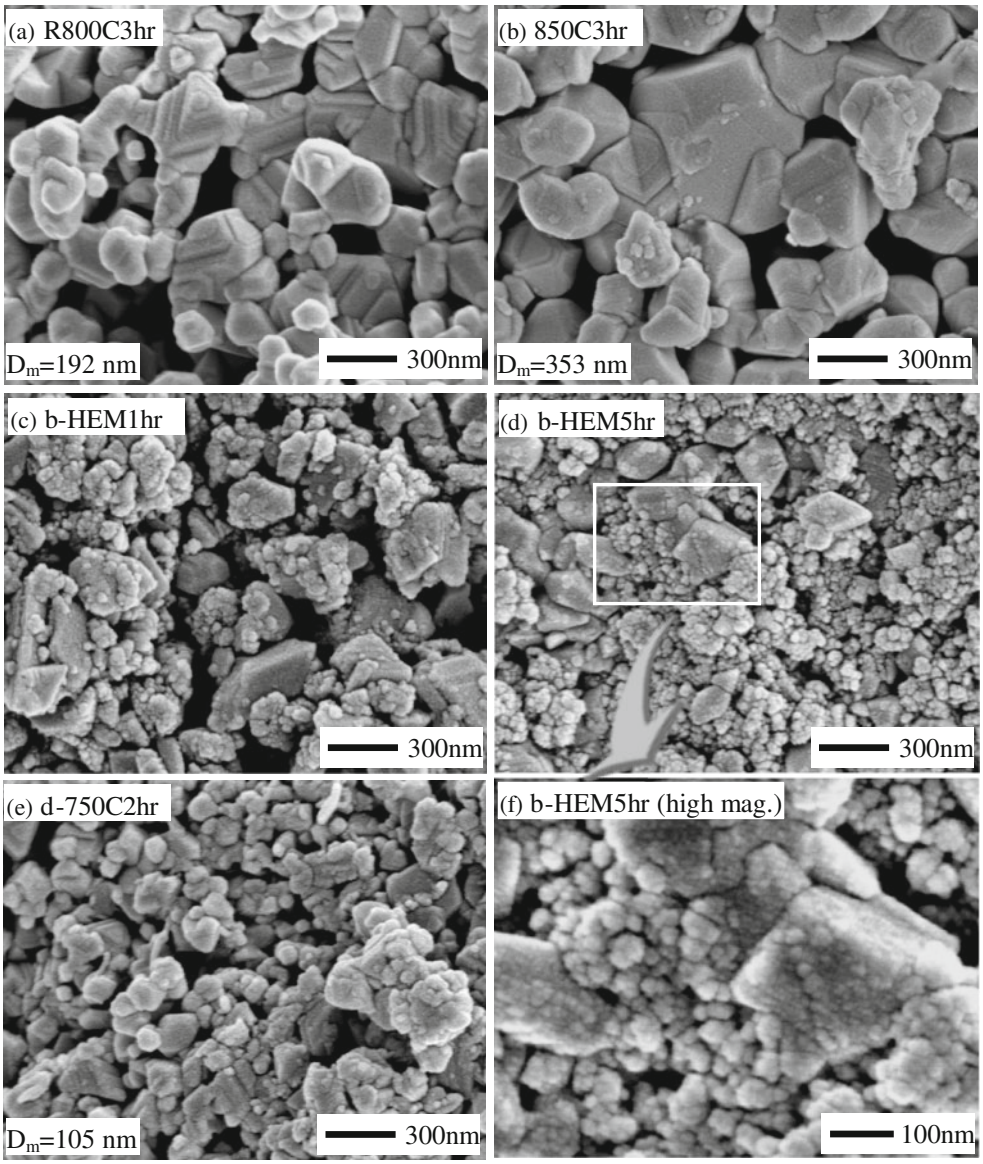

Fig. 2 SEM images of the $Li_4Ti_5O_{12}$ samples prepared in this study, where figure (**f**) shows the magnified image of (**d**)

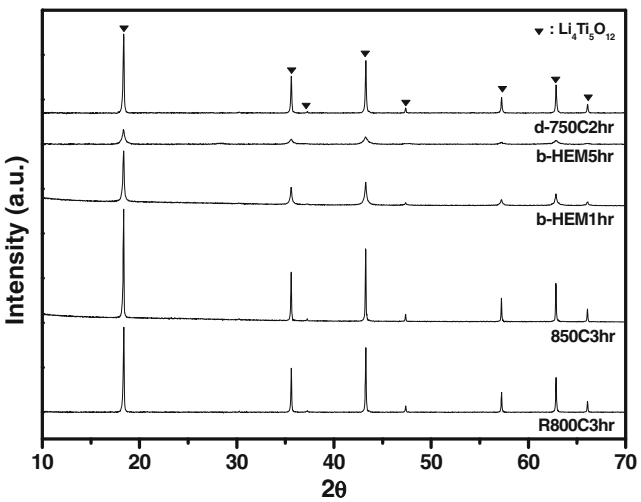

Fig. 3 XRD patterns of $Li_4Ti_5O_{12}$ synthesized by various treatments

presence of an unwanted rutile TiO_2 phase in the final $Li_4Ti_5O_{12}$ has been reported [24, 28, 29]. It is estimated that the high energy milling for the starting materials played an important role in acquiring a pure $Li_4Ti_5O_{12}$ because of the decreased diffusion length required to complete a solid-state reaction. Even though all samples showed pure $Li_4Ti_5O_{12}$, the peak height varied significantly depending on the treatment. The samples synthesized by heat treatment at 800 and 850°C showed sharp XRD peaks, indicating the highly crystalline nature of these particles. On the other hand, the peak heights decreased significantly by 1 and 5 h of high energy milling due to the decrease in crystallinity, and increased again by annealing at 750°C for 2 h. Since XRD can only detect the existence of crystalline phases, Raman spectra were taken to examine the evolution of amorphous TiO_2 and/or Li_2CO_3 upon milling. According to the Raman spectra shown in Fig. 4, all samples showed the characteristic peaks

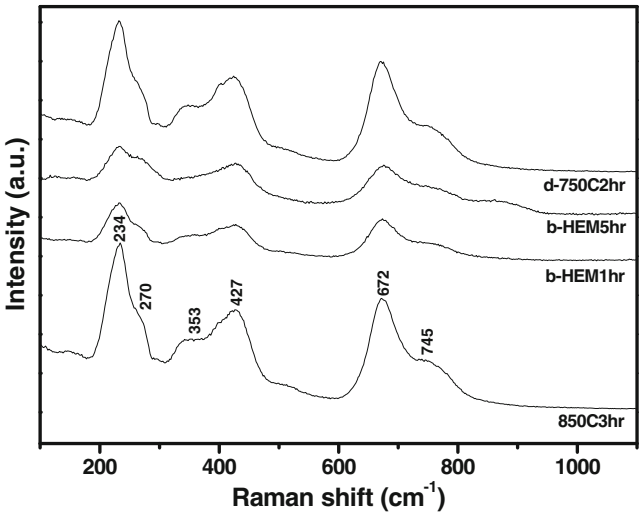

Fig. 4 Raman spectra of $Li_4Ti_5O_{12}$ synthesized by heat treatment, post-milling and subsequent annealing

of $Li_4Ti_5O_{12}$, even though the peak height was decreased with the high energy-milled samples. The peaks at 672 and 745 cm^{-1} are assigned to the A_{1g} mode, and the broad peak at 427 cm^{-1} is assigned to the E_g mode. The 3 peaks at 234, 270 and 353 cm^{-1} are assigned to the F_{2g} modes, which are in good agreement with those reported in the literature [30, 31]. Therefore, it can be concluded that the crystallinity of $Li_4Ti_5O_{12}$ was decreased significantly by high energy milling without generating any second phases.

Figure 5 shows the galvanostatic charge/discharge profiles at 0.1 *C* in the third cycle for the half-cell prepared using various $Li_4Ti_5O_{12}$ samples. It can be found that the lithium extraction capacity of $Li_4Ti_5O_{12}$ electrodes depends significantly on the post-treatments, such as milling and annealing. For example, the specific capacities of R800C3hr and 850C3hr were 152 and 155 $mAhg^{-1}$, respectively, whereas those for high energy-milled b-HEM1hr and b-HEM5hr decreased to 145 and 128 $mAhg^{-1}$, respectively. The lowest capacity of b-HEM5hr was increased to 147 $mAhg^{-1}$ from 128 $mAhg^{-1}$ by 2 h of annealing at 750°C. In addition, the polarization, which is proportional to the gap between the charge and discharge curves, increased by high energy milling and decreased by the subsequent annealing. The heat-treated samples, such as R800C3hr, 850C3hr and d-750C2hr, showed a flat voltage profile due to the two-phase reaction, which is the typical behavior of a crystalline $Li_4Ti_5O_{12}$ [32]. On the other hand, the flat plateau of the voltage profile was decreased drastically by high energy milling, as shown with the b-HEM1hr and b-HEM-5hr samples in Fig. 5. This curved voltage profiles with the high energy milled $Li_4Ti_5O_{12}$ samples may be attributed to the one phase reaction of the amorphous phase or the formation of solid solution between $Li_4Ti_5O_{12}$ and $Li_{4+x}Ti_5O_{12}$ ($0<x<3$), as reported in $LiMn_2O_4$ [33] Therefore, it is believed that the decrease in capacity and plateau associated with high energy milling is mainly related to the decrease in the crystallinity of $Li_4Ti_5O_{12}$.

Figure 6 (a) and (b) show the cyclic performance and normalized capacity at the third cycle as a function of the *C*-rates, respectively. The *C*-rates were varied in the order of 0.1 – 0.2 – 0.5 – 1.0 – 2.0 – 5.0 – 10.0 – 0.1 *C* with 3 cycles at each rate and a rest time of 10 min after each measurement. Although most of the samples showed good cyclability at each *C*-rate along with the complete capacity recovery to the initial value at the final 0.1 *C*, the rate capability depends on the type of samples, as shown in Fig. 6 (a). The rate capability, which is defined as the ratio of discharge capacity at a corresponding C-rate with respect to that at 0.1

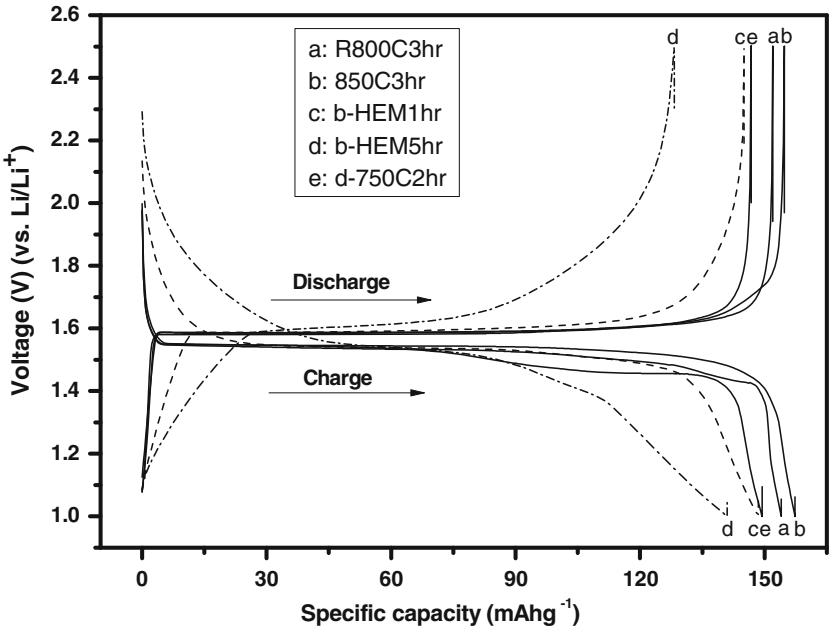

Fig. 5 Voltage profiles for charge and discharge of $Li_4Ti_5O_{12}$ electrodes prepared by different treatments at third cycle with the rate of 0.1 *C*

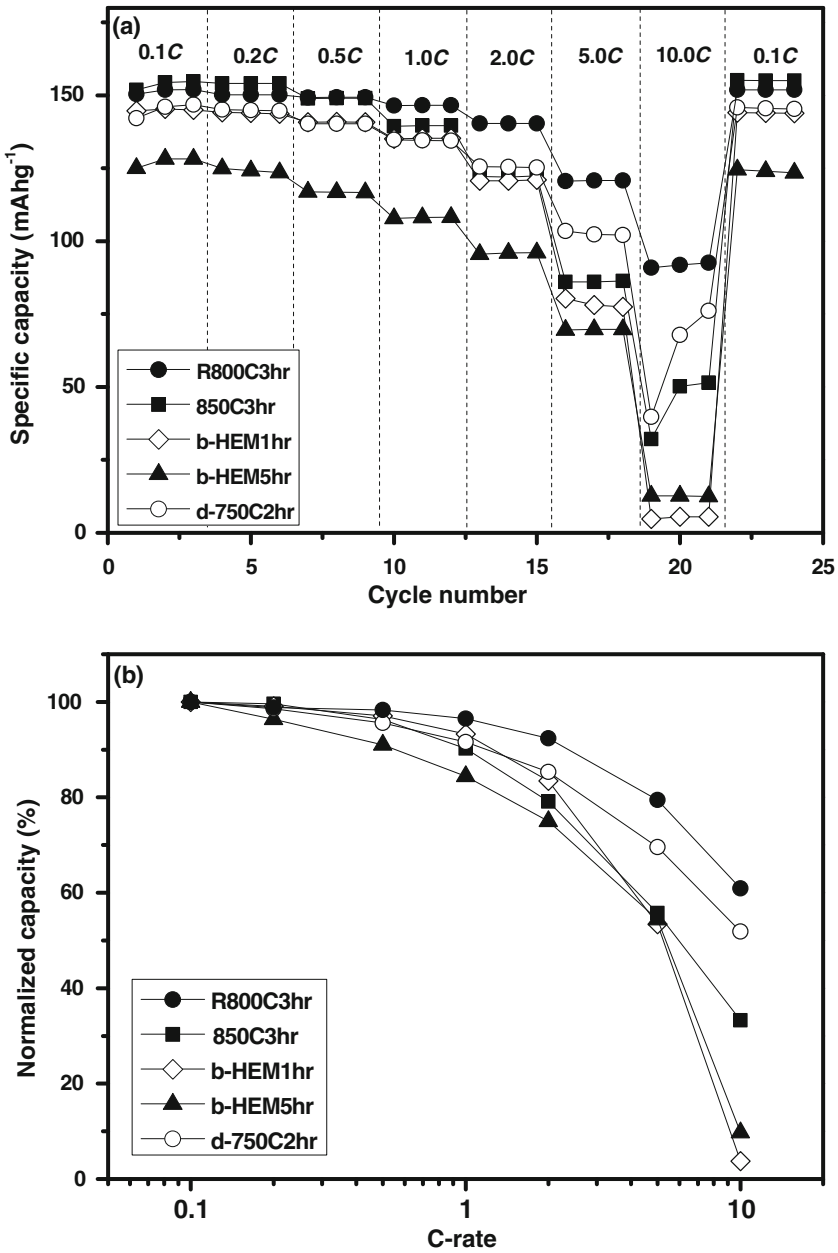

Fig. 6 (**a**) Cyclic performance and (**b**) normalized capacity as a function of the *C*-rate for $Li_4Ti_5O_{12}$ electrodes prepared by various treatments

C, of the electrodes prepared with R800C3hr appeared to be the best of all the *C*-rates among all samples, as shown in Fig. 6 (b), due to their relatively fine particle size and high crystallinity. On the other hand, the rate capabilities of the samples prepared by the high energy-milled $Li_4Ti_5O_{12}$ were deteriorated significantly compared to that of the R800C3hr sample in spite of their finer particle sizes. One notable aspect is the recovery in rate capability of the annealed d-750C2hr sample for all of the *C*-rates, which is similar to the capacity behavior shown in Fig. 5. The rate capability of d-750C2hr was significantly better than those of the 850C3hr and high energy-milled samples, even though it was still slightly lower than that of R800C3hr. For example, the normalized capacities at 5 *C* with respect to those at 0.1 *C* for R800C3hr, 850C3hr, b-HEM1hr, b-HEM5hr and d-750C2hr were 79, 56, 54, 54 and 70 %, respectively, while decreasing to 61, 33, 4, 10 and 52 % at 10 *C*. The normalized 70 % capacity for d-750C2hr at 5 *C* was shown to be comparable or even better than those prepared by wet chemical routes. Yuan et al. [23, 24] reported the normalized capacities of 56–78 % for the $Li_4Ti_5O_{12}$ synthesized by a cellulose-assisted combustion process, while Woo et al. [25] reported 46 % capacity using a colloidal crystal templating process at the same *C*-rates. The better rate capability of d-750C2hr than that of the 850C3hr sample, in spite of its lower capacity as shown in Fig. 5, seemed to be attributed to the finer particle size which promotes the Li^+ intercalation and de-intercalation process through the short diffusion path

and enhanced contact area between $Li_4Ti_5O_{12}$ and the electrolyte. These overall results indicate that the crystallinity of $Li_4Ti_5O_{12}$ is an important factor for achieving a high capacity and rate capability, in addition to the fine particle size.

4 Conclusions

This study examined the possibility of nano-sized $Li_4Ti_5O_{12}$ synthesis from a coarse solid-state reacted powder by high energy milling as well as its electrochemical properties for lithium ion battery applications. After solid-state synthesis of $Li_4Ti_5O_{12}$ using Li_2CO_3 and TiO_2 by heat treatment at 800 and 850°C for 3 h, the sample treated at 850°C was exposed to 1 and 5 h of high energy milling, while the powder treated at 800°C was used as a reference sample. Although the mean particle size of 25 nm could be achieved by 5 h of milling, the crystallinity of the milled $Li_4Ti_5O_{12}$ was decreased drastically due to the damage associated with the milling, without generating any second phase. The electrochemical properties of the milled powder were decreased significantly compared to those with powder treated at 800°C without milling. However, it was observed that both the decreased capacity and rate capability for the milled powder could be recovered by a subsequent annealing at 750°C due to the increase in particle crystallinity. These results suggest that the $Li_4Ti_5O_{12}$ crystallinity is also an important factor in the enhancement of the electrochemical properties, in addition to the fine particle size. More detailed study on the optimization of high energy milling and subsequent annealing using solid-state $Li_4Ti_5O_{12}$ is currently in progress to replace the expensive wet chemical routes for the economic synthesis of nano-sized anode material for high power applications of $Li_4Ti_5O_{12}$-based lithium ion batteries.

Acknowledgements This research was supported by the Industrial Core Technology Program funded by The Ministry of the Knowledge Economy, Republic of Korea. (Project No. 10035302)

References

1. B. Scrosati, J. Garche, J. Power Sources **195**, 2419 (2010)
2. A.K. Shukla, T.P. Kumar, Curr. Sci. **94**, 314 (2008)
3. M. Winter, J.O. Besenhard, M.E. Spahr, P. Novak, Adv. Mater. **10**, 725 (1998)
4. R.F. Nelson, J. Power Sources **91**, 2 (2000)
5. B. Scrosati, Nature **373**, 557 (1995)
6. K.M. Colbow, J.R. Dahn, R.R. Haering, J. Power Sources **26**, 397 (1989)
7. K. Zaghib, M. Armand, M. Gauthier, J. Electrochem. Soc. **145**, 3135 (1998)
8. A. Guerfi, S. Sévigny, M. Lagacé, P. Hovington, K. Kinoshita, K. Zaghib, J. Power Sources **119–121**, 88 (2003)
9. G. Wang, J. Xu, M. Wen, R. Cai, R. Ran, Z. Shao, Solid State Ionics **179**, 946 (2008)
10. A. Guerfi, P. Charest, K. Kinoshita, M. Perrier, K. Zaghib, J. Power Sources **126**, 163 (2004)
11. T. Ohzuku, A. Ueda, N. Yamamoto, J. Electrochem. Soc. **142**, 1431 (1995)
12. K. Hsiao, S. Liao, J. Chen, Electrochimica Acta **53**, 7242 (2008)
13. D. Aurbach, E. Zinigrad, Y. Cohen, H. Teller, Solid State Ionics **148**, 405 (2002)
14. W.J. Zhang, J. Power Sources **196**, 13 (2011)
15. J.C. Arrebola, A. Caballero, L. Hernán, Nonotechnology **18**, 295705 (2007)
16. A.D. Pasquier, C.C. Huang, T. Spitler, J. Power Sources **186**, 508 (2009)
17. L. Kavan, J. Procházka, T. Spitler, M. Kalváč, M. Zukalová, T. Drezen, M. Grätzel, J. Electrochem. Soc. **150**, A1000 (2003)
18. J.L. Allen, T.R. Jow, J. Wolfenstine, J. Power Sources **159**, 1340 (2006)
19. J. Li, Z. Tang, Z. Zhang, Electrochem. Commun. **7**, 894 (2005)
20. S.Y. Yin, L. Song, X.Y. Wang, M.F. Zhang, K.L. Zhang, Y.X. Zhang, Electrochimica Acta **54**, 5629 (2009)
21. T. Yuan, R. Cai, K. Wang, R. Ran, S. Liu, Z. Shao, Ceram. Int. **35**, 1757 (2009)
22. N.A. Alias, M.Z. Kufian, L.P. Teo, S.R. Majid, A.K. Arof, J. Alloys Compd. **486**, 645 (2009)
23. T. Yuan, R. Cai, P. Gu, Z. Shao, J. Power Sources **195**, 2883 (2010)
24. T. Yuan, R. Cai, R. Ran, Y. Zhou, Z. Shao, J. Alloys Compd. **505**, 367 (2010)
25. S.W. Woo, K. Dokko, K. Kanamura, Electrochimica Acta **53**, 79 (2007)
26. S.S. Ryu, D.H. Yoon, J. Mater. Sci. **42**, 7093 (2007)
27. D.H. Yoon, J. Ceram. Proc. Res. **7**, 343 (2006)
28. E. Matsui, Y. Abe, M. Senna, A. Guerfi, K. Zaghib, J. Am. Ceram. Soc. **91**, 1522 (2008)
29. J. Li, Y.L. Jin, X.G. Zhang, H. Yang, Solid State Ionics **178**, 1590 (2007)
30. C.M. Julien, K. Zaghib, Electrochim. Acta **50**, 411 (2004)
31. L. Aldon, P. Kubiak, M. Womes, J.C. Jumas, J. Oliver-Fourcade, J.L. Tirado, J.I. Corredor, C.P. Vincente, Chem. Mater. **16**, 5721 (2004)
32. M. Wagemaker, D.R. Simon, E.M. Kelder, J. Schoonman, C. Ringpfeil, U. Haake, D. Lützenkirchen-Hecht, R. Frahm, F.M. Mulder, Adv. Mater. **18**, 3169 (2006)
33. M. Okubo, Y. Mizuno, H. Yamada, J. Kim, E. Hosono, H. Zhou, T. Kudo, I. Honma, ACS Nano **4**, 741 (2010)